# Assessment of biomass and biochar as a porous medium for water retention in soils

Rodrigo Vieira Santos
vieira.santos@tecnico.ulisboa.pt

Instituto Superior Técnico, Universidade de Lisboa, Portugal

December 2021

## Abstract

Biomass and its by-products, namely biochar are research objective due to the variety of applications they can have, being mainly due to its porous structure, as the increase of water in soils. It was proposed to evaluate this effect, using two biomasses (pine and eucalyptus), their respective biochars and activated biochars, produced in two different scales, laboratory pine and industrial eucalyptus. Through the characterisation of the materials (BET, Mercury Porosimetry, SEM and TGA) it was observed that both biomasses have a similar thermal decomposition and that the activation has a significant effect on the specific area, 937 m2g-1 and 112 m2g-1 for pine and eucalyptus. While for larger pores, it is found that the pores of the original biological structure have a great influence for the structure of their biochars. SEM images proved elongated pores and that pine has pores in a larger range than eucalyptus. Although the greatest moisture adsorption was in activated pine, due to the CO2 activated sites, both biomasses also exhibited considerable appetence due to the surface functional groups. A correlation (r=0.95) was found between the total pore volume and the water holding capacity. Regarding water retention curves, in the various mixtures with sand (10%,50% biomass/biochar by volume), an increase in retention was found for plant-available water (maximum observed 50%). For biochars, it is due to their intraporosity, and it is found that smaller pores retain water for higher pressures. For mixtures of 10% the biomasses show a higher increase than the biochars

**Keywords:** biomass, biochar, slow pyrolysis, specific area, porosity, water retention

## 1. Introduction

Biomass is a versatile material that has always been used by the human being, however, due to the challenges that modern society has been implementing both to the planet and to the human being, the increase of research and the use of biomass has gained relevance again. It can be an instrumental element of energy security and sustainable development, however biomass and their products through conversion processes have a lot of applications beyond energy use, thus making it a resource with enormous scientific and economic potential that has been the subject of much research over the years. [1]

Raw biomass itself has certain disadvantages, such as low energy density and the inconvenience in the form of biomass that can be difficult to handle, store and transport. All this has led to the conversion processes taking a major role, since transforming solid biomass into liquid, gaseous and solid fuels (with better properties) would make it easier to handle this type of fuel. [2] And precisely one of the processes that is the target of research is pyrolysis, since they have a by-product that has several applications.[3] This thermochemical processes involve complex reactions and depend on various parameters such as temperature, residence time, heat-rate, pressure, type of biomass and type of reactors [3],[4]. One outcome of these processes is biochar[5], which is a product that, if obtained under certain specific parameters, may have several applications, namely through its porous structure[6], besides being associated with carbon sequestration.[7]

The major applications for biochar are solid fuels, soil amendment and activated carbon. Some studies have shown that the high heating rates favour the formation of pore in pyrolysis biochars and following the correct operating conditions biochar may be produced with favourable BET surface area, high adsorption properties and high combustion reactivity[8],[9]. Therefore, biochar as a porous structure can have a considerable effect on soils, namely on desertified (sand-based) soils, where the capacity to retain water and nutrients is low and therefore plants have difficulties to survive. In China there are large areas where plants and crops cannot thrive due to water storage, severe droughts due to climate change result in the degradation of these soils, i.e., desertification and sandification, consequently increasing water loss through evaporation and decreasing the water retention capacity of the soils on these lands.[10] In addition, this soil improvement can be done chemically, studies show that incorporation of biochar into soils increases soil pH, cation exchange capacity and the amount of extractable nutrients such as Ca, Mg, K and Na, which are beneficial for soil fertility and nutrient retention[11]. And physics in a direct way, in which the biochar as a porous structure retains water in its pores and then increases the soil water content. Or the indirect way in which the biochar added with the soil will bind with other constituents improving the soil structure which increases the amount of water in soil[12]. So, to understand water retention in soils and how this can have a positive influence on the amount of water available to plants for example, it is necessary to understand the mechanisms by which they retain water. It is also important to study their ability of moisture sportion since biomass and biochar are hygroscopic materials.

Thus, in this work, an analysis was made of two types of woody biomass and their biochars (resulting from slow pyrolysis), being produced by different processes (laboratory and industrial). Both materials were characterized, with special focus on the porous structure. To evaluate the performance of the materials, moisture equilibrium curves, water holding capacity tests and water retention curves were performed by mixing the different elements with sand (varying the percentage used) in order to assess the capacity of the materials as a function of their structure. Section 1 presents an introduction related to the topic under study. Section 2 gives an overview of the methods used in the work. In section 3 the main results are presented and discussed. Finally, in section 4 and 5 the conclusions and references are stated.

## 2. Materials and Methods

This chapter includes the experimental procedures used in this work concerning biochar production (two types of process), physical activation of the biochar, characterization of the biomass and biochar and three tests related to moisture adsorption and water retention.

### 2.1. Biomass

The biomasses used in this work are woody biomass: Pine Sawdust ("Pinus"), Eucalyptus ("Eucalyptus Globulus"). The Pine Sawdust was supplied by the IDMEC Laboratory (Mechanical Engineering Institute – IST) and the Eucalyptus was obtained on an industrial scale supplied by the company Bio Green Woods®. They were dried for 24 hours and sieved to obtain a particle size in the range 400-1000 µm. Following the standards USP General Test 768 Method I and ISO 3310. In relation to the tests involving mixtures, the type of sand used is a silica-based sand and follows the same standards mentioned. Table 1 represents the breakdown by volume percentage used in the tests between biomass/biochar and sand. In terms of nomenclature PS- Raw is used for pine sawdust biomass, PS-C600 for pine biochar produced at 600 ºC, PS-AC for activated pine biochar, EU-Raw for eucalyptus biomass, EU-C550 for eucalyptus biochar at 550 and EU-AC for activated eucalyptus.

**Table 1-** Breakdown of the percentages by volume used between biomass/biochar and sand

| Test | Biomass/biochar [% Volume] | Sand [% Volume] |
|---|---|---|
| **Equilibrium Moisture content** | 100% | - |
| **Water holding Capacity** | - | 100% |
| | 100% | - |
| **Water Retention curves** | 50% | 50% |
| | 10% | 90% |

### 2.2. Methods

The methodology of the work is divided into several parts, such as the materials used (two types of woody biomass), the processes used (batch/laboratory and continuous/industrial), the characterization methods (proximate analysis, thermogravimetric analysis, Scanning Electron Microscopy analysis, Brunauer-Emmet-Teller (BET) and Mercury Porosimetry), the evaluation tests (equilibrium moisture content, water holding capacity and water retention test) and finally the parametric models. These tests were carried out according to the percentages of table 1 in order to assess the influence of the percentage on the results.

#### 2.2.1. Biochar Production

The biochar production processes used are different, one is batch and has been controlled in laboratory while on the other hand the second one is done continuously and controlled industrially by Bio Green Woods®. Experimental setup is shown in figure 1. It consists of a horizontal reactor of controlled atmosphere with constant volume and the internal tube is made of alumina having an internal diameter of 4 cm and a length of 55 cm. Heating is done by an electrical resistance, being controlled by the Eurotherm 3216 controller. In terms of procedure, the biomass is placed in the crucibles positioning them in the central position of the tube, then purged with the carrier gas N2, the heating rate used is 33ºC/min and the residence time 1 hour. The biomass used was pine sawdust and the temperature range was between 300ºC and 600ºC, since the offset in surface area occurs around 500ºC.[3] To produce an activated biochar, a physical activation was performed introducing a $CO_2$ flow rate of 104 mL/min during 1 hour. Subsequently the mass yield, $Ym$ was determined with equation 1:

$$Ym = \frac{m_{final}}{m_{initial}} \quad (1)$$

Where $m_{final}$ is the mass of the biochar obtained and $m_{initial}$ is the mass of raw biomass.
The industrial process was carried out by the company, using a continuous production reactor, namely screw pyrolizer. For this work two types of materials were supplied, the first one a biochar produced at a temperature of 550 ºC and the second one an activated biochar. The information in relation to the other parameters was not provided by the company.

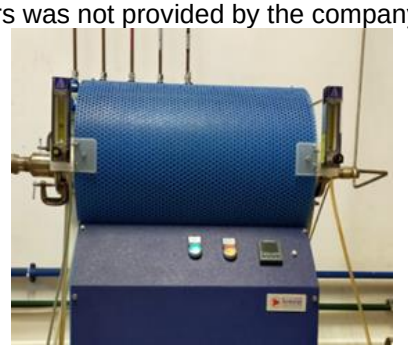

**Figure 1-**Horizontal heating furnace

### 2.2.2. Characterization of material

Biomass and biochar are characterized by its composition, thermal decomposition, surface topography, surface area and porosity.

#### 2.2.2.1. Proximate Analysis

Proximate Analysis gives the composition in terms of gross components such as Moisture (M), volatile matter (VM), ash (ASH) and fixed carbon (FC). These elements are presented in percentage. VM was determined following the standard EN 15148:2009, Ash followed standard EN ISO 18122, moisture standard EN ISO 18134-3 and fixed carbon is computed by difference of the remaining components. Furthermore, in order to assess the possibility of using the material as a fuel, a correlation, proposed by Parikh et.al. [13]:

$$HVV[MJ/kg] = 0.3536FC\% + 0.1559VM\% - 0.0078ASH\%\ [dry-basis] \quad (2)$$

#### 2.2.2.2. Thermogravimetric analysis

The thermogravimetric analysis was performed in Perkin Elmer STA 6000 Simultaneous Thermal Analyzer. The thermogravimetric (TG) curves show the sample weight loss as a function of temperature and the derivative (DTG) curves show the rate of weight loss with temperature. Each sample was analysed at least three times, and the average values were considered. To analyse the data was used a moving average with a 60 period.

#### 2.2.2.3. SEM

Morphology and chemical composition of biomass and biochars were analysed using a scanning electron microscope (SEM), the instrument used was JEOL model JSM-7001F. This analysis are used to evaluate the morphologic of the biochar particles after different treatments as well as the raw biomasses.

#### 2.2.2.4. Brunauer-Emmett-Teller (BET)

In this work to determine the surface area of the samples (through the physical of gas adsorption) and their isotherms the following equipments were used: Quantachrome model Autosorb iQ (Kr at 77K) and Quadrasorb ($N_2$ at 77K) equipped with vacuum systems with termolecular pumps. In terms of experimental conditions, degasification was previously carried out in vacuum, with a thermo molecular pump, for 3 days at ambient temperature followed by 4h at 60 ºC (biomass) and 8h at 200 ºC (biochar), with a heating ramp of 2ºC/min until the final temperature. The specific areas were determined from the adsorption of N2 at 77k, except for the raw biomass that was determined through Kr at 77K (it presents a low area not being possible to obtain a result with N2), following the recommendations of IUPAC.

#### 2.2.2.5. Mercury Porosimetry

This method was used to obtain various aspects of the porous structure such as pore diameter, pore size distribution, total pore volume, surface area and absolute and bulk density. AutoPore® IV 9500 Series was the instrument used. This equipment has a range of low pressure between 0 to 345 kPa, which translates to pore size range of 360 to 3.6 µm and a range of high pressure between atmospheric pressure to 228 MPa, corresponding to 6 to 0.003 µm.

#### 2.2.2.6. FTIR

Fourier transform infrared spectroscopy was performed using PerkinElmer spectrum two FT-IR spectrometer which thus allows obtaining a curve of transmittance/absorbance as a function of wavenumber and consequently through the peaks of this curve it is possible to identify the functional groups present on the surface of the material.

### 2.2.3. Equilibrium Moisture Content curves

As biomass and biochar are hygroscopic materials, to assess their adsorption capacity, a moisture adsorption test was carried out. Therefore, to evaluate the transient behaviour in moisture adsorption of the different samples, the following method was elaborated: After drying the samples for 24 hours at 105 ºC in an oven, a constant volume, 4 cm3, of sample was measured in a 10 cm3 volumetric cylinder with a precision of 0.1 cm3. Then the sample is spread evenly on a petri dish surface (also dried and placed in a desiccator) with a diameter of 70 mm and a height of 15 mm and is placed back in the oven for 1h. After this time, it is weighed and placed again for 1h in the oven until the difference between weighing is less than 0.1 mg. Ensuring that the sample is completely dry, it is placed in a closed room with a hygrometer and the variation in mass is determined using a KERN ABT 120-5DM precision balance (accuracy of 0.01 mg), first at 15 min intervals, then at 30 min intervals and finally at 1h intervals until a difference of less than 0.1 mg is recorded, thus reaching the equilibrium. The temperature and relative humidity values are monitored throughout the test using the hygrometer and the test is only valid if they remain constant at all times.

### 2.2.4. Water Holding Capacity

For measurement of water holding capacity (WHC) of the studied samples with different physical structure, a constant volume of sample ,12 cm3, was placed in an acrylic tube with a diameter of 32 mm, a height of 50 mm and with one end covered with a wire mesh reduced in size so as not to allow particle of less than 400 microns to pass through, allowing total water permeability. Then the tube with the sample is imbibed in a glass beaker with deionized water for 24 hours. The direction of the water is upwards (imbibition) and slow enough not to cause changes in the structure of the materials. The sample with the tube is then fixed in a bigger container in order to let excessive water drain for about 15 min (i.e., until there is no more dripping from the sample). Wet sample is then weighted and consequently dried in an oven at 105 ºC until no more wight loss is registered. Similar methods has been reported in the literature [12],[14]. Water holding capacity is computed by using equation 3:

$$WHC(cm^3/cm^3) = \frac{(M_1 - M_2)/\rho_w}{V_s} \quad (3)$$

Where $M_1[g], M_2[g], \rho_w \left[\frac{g}{cm^3}\right] V_s[cm^3]$, are total weight of wet sample and acrylic tube, total weight of dry sample and acrylic tube, density of water and volume of sample, respectively.

### 2.2.5. Water Retention Curves (pF curves)

#### 2.2.5.1. The experimental approach

The water retention curves were obtained for different points of matric or capillary potential: saturation point (ψ = 0 kPa), field capacity points (ψ = 10 kPa and ψ = 33 kPa) and wilting point (ψ = 1500 kPa). It is common to present these values in logarithmic form through the following equation:

$$pF = \log\ (\psi) \qquad (4)$$

With ψ , the pressure applied in hPa. Then on pF scale the points that are calculated are the saturation, pF 2.0 (field capacity), 2.5 and 4.2 (wilting point). Different apparatus were used to measure the different pressure points. For the saturation point and for 10 kPa (pF 2) a sand suction table (figure 2) was used. While for the points of 33 kPa and 15000 kPa a ceramic pressure vessel with a ceramic plate and regulated air system used to control the pressure inside the vessel (figure 3).

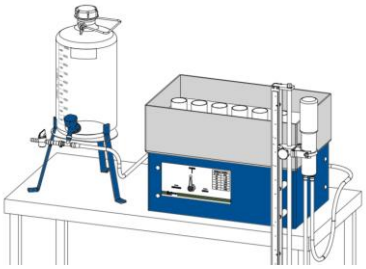

**Figure 2 –** Sandbox for pF-determination

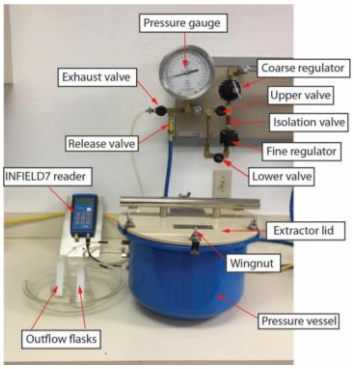


**Figure 3 –** Pressure vessel using a regulated air system.[15]

The water content (θ) is then calculated as follows:

$$\theta_i \left[\frac{cm^3}{cm^3}\right] = \frac{(m_{wi} - m_{dry})/\rho_w}{V_{ring}} \qquad (5)$$

Where,$m_{wi}[g], m_{dry,}[g], \rho_w[g/cm^3], V_{ring}[cm^3]$ represents the mass of wet sample at each applied pressure, the mass of oven dry sample, the density of deionized water (1 g/cm$^3$) and the volume of the sample ring.

#### 2.2.5.2. Van Genutchen Model

To estimate the water retention curves, is used an empirical model called Van Genutchen Model[16]. It is a one-dimensional model that relates soil water content with soil water potentials and is given by:

$$\theta(\psi) = \theta_r + (\theta_s - \theta_r) \cdot \left[\frac{1}{(1 + (\alpha|\psi|)^n}\right]^{1-\frac{1}{n}} \qquad (6)$$

Where $\theta(\psi)[\frac{cm^3}{cm^3}]$ is the volumetric water content at given matric potential $\psi$ , $\theta_s \left[\frac{cm^3}{cm^3}\right]$ is the saturated water content when $\psi = 0$ , $\theta_r$ is the residual water content $[\frac{cm^3}{cm^3}]$ and $\alpha$ and n are shape parameters, representing the inverse of the entry pressure and the pore size distribution, respectively.

### 2.2.6. Statistical Analysis

All the measurements were repeated at least three types to ensure reproducibility of results and were done at the same time to ensure the same conditions. Standard deviation was also calculated and represented in the graphs with error bars. Pearson correlation was used to correlate variables. And non-linear least squares method to equation fitting with the experimental data.

## 3. Results and Discussion

### 3.1 Biochar Production

The curve representing the mass yield of the laboratory process for biomass carbonization at an electrically heated horizontal tube furnace is shown in figure 4. As expected, a reduction in the mass yield is observed with the temperature increase, due to the release of condensable, tars and non-condensable gases due to the breakdown of the various constituents of the pine biomass. There was a reduction from 38.47% to 20.11%, for 200 ºC and 600 ºC, respectively. However, there is a more significant reduction between 300 ºC and 400 ºC of 12.78% than between 400 ºC and 500 ºC of only 4,94%.%. This is explained by the fact that pine is a lignocellulosic biomass with its composition being mostly based on cellulose, hemicellulose and lignin and by analysing the thermodecomposition of these constituents it is found that cellulose decomposes mostly around 380 ºC, hemicellulose around 300 ºC and lignin gradually decomposes throughout the temperature range. In the production of activated carbon through biochar at 600 ºC, the mass yield obtained was 11.79% with a standard deviation of 1.16%.

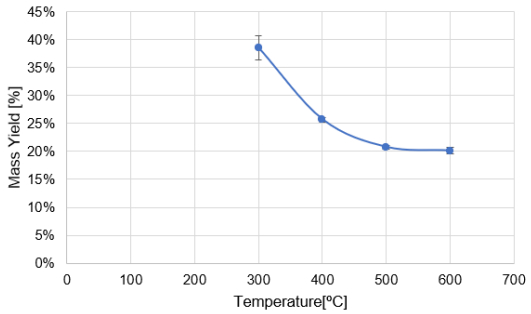


**Figure 4-** Mass yield curve for a temperature range from 300ºC to 600ºC for Pine Biomass.

### 3.2. Characterization of laboratory and industrial biomass and biochar

#### 3.2.1. Proximate, thermogravimetric and hydrophobicity analysis

Since most biomasses are hygroscopic it is important to represent the approximate analysis on a dry basis. Table 2 shows the results for the studied materials in these conditions. Both PS-Raw and EU-Raw present high values of volatile matter (86.85% and 88.34%), meaning that they may have the ability to release a lot of gases during the thermochemical processes in which they are involved. Among the obtained biochars, both have a considerably high value of fixed carbon, since the carbonization process has as one of the main objectives that fixation of carbon. Although the differences are not very distinct, the PS-C600 was the one which presented a lower volatile matter (15.16%) and higher ash content (1.39%), while EU-C550 carries the highest percentage of volatiles (18,89%). This proves that the processes used are different and that the conditions used in the production of EU-C550 do not maximise the volatiles release. However, comparing with EU-AC, it is possible to see an improvement in the process in order to obtain a biochar with less volatile matter and a higher carbon fixation (18.32 % and 81.23%). To clarify the devolatilization process and to support the data obtained in the proximate analysis, a thermogravimetry and the corresponding derivative curves (figure 5) were performed. Considering biomass, the largest mass variation occurs between 300 and 400ºC, due to the release of volatiles and comparing with the decomposition of hemicellulose and cellulose (which are the major constituents of pine and eucalyptus) the largest mass variation occurs between 250ºC and 350ºC, so this variation is due precisely to the influence of their constituents. For biochars, the mass variation occurs close to the process temperature, highlighting the variation of EU-C550 that would be expected to occur earlier, since it is an industrial process, in which carbonization may not always be complete. It is necessary to bear in mind that pyrolysis is a complex process, depending on several parameters.

Figure 6 depicts the transmittance curves for the various wavelengths for pine biomass and its biochars. For PS Raw there is a broad transmittance band between 3650 and 3250 $cm^{-1}$, indicating hydrogen bond. This band confirms the existence of hydrate (H2O), hydroxyl (-OH), ammonium, or amino. A narrow band at below 3000 $cm^{-1}$ (2935 and 2860 $cm^{-1}$) is also visible, showing aliphatic compounds. Whereas the transmittance band observed between 1200 and 900 cm-1, corresponds to alcohol and hydroxy compounds (primary alcohols C-O stretch). For PS-C600 it is possible to see a considerable decrease of functional groups due to the temperature during pyrolysis. While for the activated biochar, it is not possible to conclude clearly, although functional groups are expected due to the reaction with $CO_2$.

**Table 2-** Proximate analysis for biomasses and biochars on a dry basis.

| Sample Type | Volatile Matter (%) | Ash (%) | Fixed Carbon (%) | Calorific Value [MJ/Kg] |
|---|---|---|---|---|
| **PS-Raw** | 86.85 | 0.49 | 12.66 | 18.01 |
| **EU-Raw** | 88.34 | 0.13 | 11.52 | 17.84 |
| **PS-C600** | 15.16 | 1.39 | 83.46 | 31.86 |
| **EU-C550** | 20.03 | 0.83 | 79.14 | 31.10 |
| **EU-AC** | 18.32 | 0.45 | 81.23 | 31.58 |

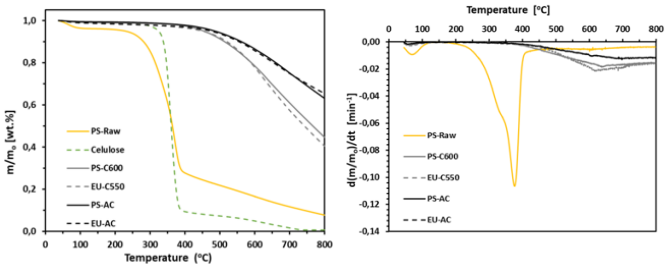


**Figure 5 –**TGA (left) and DTA (right) of PS-Raw, PS-C600, EU-C550, PS-AC and EU-AC.

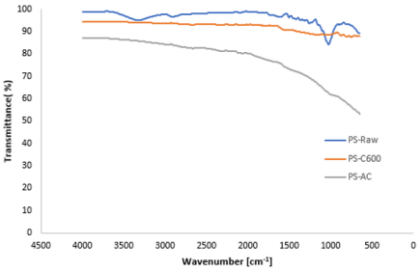


**Figure 6-** FTIR Analysis for laboratory materials.

#### 3.2.2. Porous Structure

Table 3 contains the values referring to the specific area of biomass, eucalyptus, their respective biochars and consequently the total micropore volume (within the BET test range). The average pore radius is also presented, calculated based on the total volume and surface area. To compare the evolution of the specific area through the pyrolysis process and consequently activation, the raw biomass was also tested. However, as can be seen in table 11, the value obtained was residual (0.34 $m^2g^{-1}$). Besides, it was obtained with krypton, gas that is only used for low specific areas and is not recommended by IUPAC. On the other hand, for the biochar at a temperature of 600 ºC, it shows a substantial increase in the specific area to 345 $m^2/g$, thus providing that until a temperature of 600 ºC there is an increase in the specific area of biochars. The physical activation of the pine biochar also had a considerable effect, as expected, since its specific area

increased to 937 $m^2g^{-1}$, representing an increase of 150% approximately. For Eucalyptus the same procedure was followed, however for raw Eucalyptus it was not possible to obtain a specific result since its specific surface area is very low (it is guaranteed to be lower than 5 $m^2g^{-1}$). For its biochar produced at 550 ºC a value of 20 $m^2g^{-1}$ was recorded, while for the activated correspondent a value of 120 $m^2g^{-1}$ was recorded, corresponding to an increase of 460%, representing well the activation effect. Thus, it is concluded that for both PS-C600 and PS-AC, the pyrogenic nanopores (voids that form within the carbon structure as a result of chemical changes during pyrolysis) comprise the majority of biochar surface area, and therefore provide the most sites for nutrient adsorption, cation exchange and soil microbial as well as filter contaminants from aqueous streams.[17]

To have a better model of the porous structure of both biomasses and their respective biochars, a mercury porosimetry analysis was performed, covering a range of pore size from 392 µm to 6 nm. The pore size distribution [mL/g] of both materials is represented in figure 7. Analysing the pore distribution for pine and its respective biochars, for biomass the largest amount of pores occurs for ranges from 52 µm to 10 µm, while for PS-C600 and PS-AC the largest amounts occur for ranges between 392 and 250 µm and 32 µm to 6 µm. The pore distribution between PS-C600 and PS-AC has a rather strong correlation (r=0.987), with PS-AC showing a pore range between 9 nm to 6 nm (0.006), due to activation. Between PS-C600 and PS-Raw there is a considerable correlation (r=0.734), which may indicate that most of the pores originate from the biological structure of the raw biomass. For EU-Raw, the largest amount are the larger pores (440 to 166 µm), presenting a continuous distribution throughout the whole size range. For EU-C550 and EU-AC, there is also a continuous distribution throughout the range, highlighting the peaks for 400 to 200 µm and the peak around 6.5 µm. The correlation between EU-C550 and EU-AC is high (r=0.990), as verified for pine. On the other hand, the correlation between EU-Raw and EU-C550 is intermediate (r=0.696) showing a lower value than in the case of pine, however the hypothesis of most pores coming from the biological structure is maintained [12]. Table 4, shows the total pore volume that is related to porosity, being clear that materials from pine have a higher porosity, being the maximum by PS-AC.

Through the SEM images, with a resolution of 100 µm (therefore only macro-pores are observed), present in figure 8 and 9, it can be seen that the pores have an elongated structure with different sections, both circular and rectangular. However, for pine (figure 8) it is possible to verify the hypothesis that a majority of the pores come from the biological structure of the raw biomass, since the similarity between the various figures is visible. On the other hand, in eucalyptus (figure 9) it is also possible to see the similarity between the various figures, observing in figure d) clogging in the pores in EU-raw, which may justify the difference in the previous correlation with its biochar. Finally, it is also visible that for the macro pore range, pine materials have relatively larger pores than eucalyptus, which agrees with the mercury porosimetry results.

**Table 3-** Specific areas, micropore volume and pore radius of biomass and biochars

| Sample | $A_{BET}$ [$m^2g^{-1}$] | $V_T$ [$cm^3g^{-1}$] | $R_p$[nm] |
|---|---|---|---|
| **PS-Raw** | 0.34 | - | - |
| **EU-Raw** | <5 | - | - |
| **PS-C600** | 375 | 0.184 | 0.981 |
| **PS-AC** | 937 | 0.443 | 0.946 |
| **EU-C550** | 20 | - | - |
| **EU-AC** | 112 | 0.073 | 1.304 |

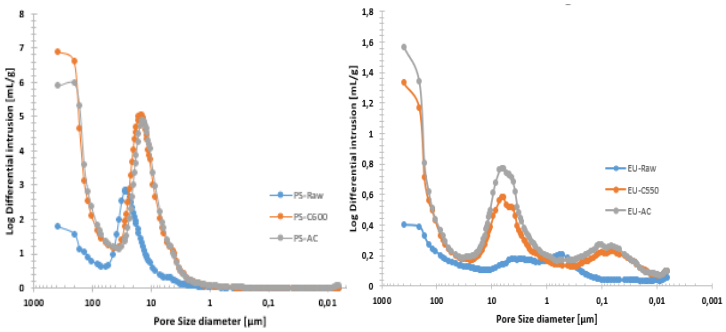


**Figure 7-**Pore size distribution for PS-Raw, PS-C600, PS-AC (left) and EU-Raw, EU-C550 and EU-AC (right)

**Table 4-** Total intrusion volume, porosity from mercury porosimetry, division between macropores and mesopores according to IUPAC, and bulk density.

| Sample | Total Pore Volume [mL/g] | Porosity [%] | Macropores (>50 nm) [mL/g] | Mesopores (2-50 nm) [mL/g] | Bulk Density [g/mL] |
|---|---|---|---|---|---|
| **PS-Raw** | 2.466 | 76.940 | 2.466 | 0.000 | 0.312 |
| **EU-Raw** | 0.669 | 51.383 | 0.636 | 0.033 | 0.769 |
| **PS-C600** | 6.631 | 88.669 | 6.631 | 0.000 | 0.134 |
| **EU-C550** | 1.509 | 68.227 | 1.394 | 0.115 | 0.452 |
| **PS-AC** | 6.372 | 88.885 | 6.366 | 0.006 | 0.140 |
| **EU-AC** | 1.797 | 69.773 | 1.678 | 0.119 | 0.388 |

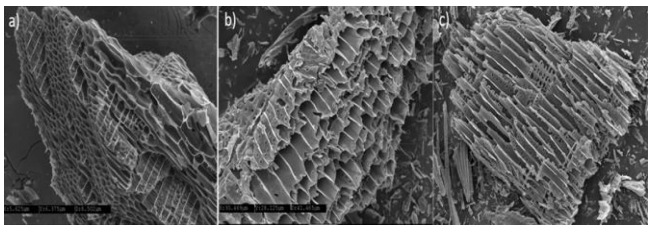


**Figure 8-**SEM images for a) PS-Raw; b) PS-C600; c) PS-AC (resolution of 100 µm)

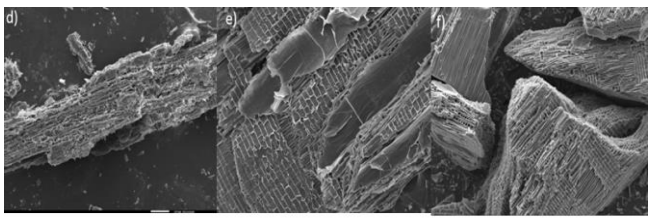


**Figure 9-** SEM images for a) EU-Raw; b) EU-C600; c) EU-AC (resolution of 100 µm)

### 3.3. Equilibrium moisture content

In this work, only one equilibrium moisture content point was considered, and the set of equilibrium moisture content points at the same temperature and different humidity corresponds to the moisture sportion isotherm, which is characteristic of each material and can only be determined experimentally. Thus, since the tests were performed at T=20ºC and RH = 70%, then it is possible to construct a graph with a point of the various moisture content isotherms for the different biomasses and biochars and make the comparison between them.

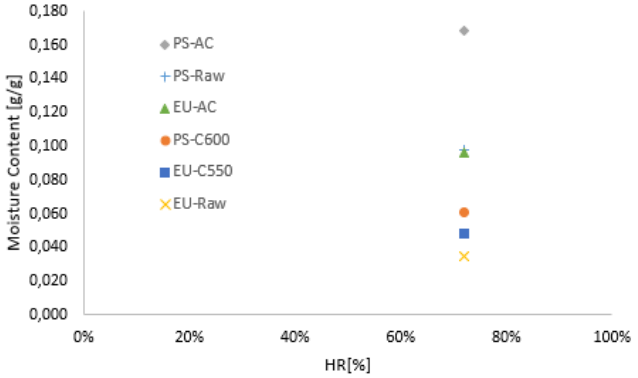


**Figure 10-** Moisture sportion isotherm experimental point for pine and eucalyptus biomasses and biochars.

Regarding the pine materials, the PS-AC is the one with the highest value (0.168 g/g).It would be expected since being an activated carbon it would have activated sites that provide a higher adsorption. Furthermore, in table 4 where the pore volume distribution by IUPAC classification is shown, it can be seen that PS-AC has 0.006 mL/g of mesoporosity, which leads one to consider that the phenomenon of capillary condensation may have an effect since the points shown are for a moisture content that is within the range considered for this phenomenon to happen. On the other hand, PS-Raw (0.097 g/g) and PS-C600 (0.061 g/g) have no volume in the range of mesoporosity, so the adsorption is due to its surface functionality which as present in figure 6 PS-Raw has more functional groups, hence shows higher value. On the other hand, for eucalyptus both EU-Raw, EU-C550 and EU-AC have a pore volume in mesoporosity of 0.033 mL/g, 0.115 mL/g and 0.119 mL/g, respectively. With EU-AC having the highest value of 0.096 g/g. However, it cannot be stated that it is directly correlated with mesoporosity and capillary condensation effect. Given that the Pearson correlation between moisture content and mesoporosity for these values is 0.69. In this case, the EU-Raw was the lowest value, being necessary the characterization of the surface functionality to conclude in relation to eucalyptus. Nevertheless, the Pearson correlation between the moisture content of all biochars (excluding raw biomasses) with their specific area determined by BET is 0.86. Although it is a considerable value, it should be careful to conclude that there is a positive correlation between these two parameters since only a complementary study of the functionality will make it clearer.

### 3.4. Water holding capacity

Analysing figure 11 it is possible to see the water holding capacity for the pine biomasses and their respective biochars, as well as for the sand, described in section 3, used as control. If there were no functional groups on the surfaces of the materials then their WHC would coincide with their total intrusion volume (their porosity, information in table 4).

Firstly, it is necessary to say that the particle size studied is from 1mm to 400 µm, and the maximum range of pores studied is up to 400 µm so in the table 4 it is not considered this larger range of pores that will also have an influence on WHC. However, looking at the eucalyptus results, it is possible to see that EU-AC has only slightly WHC than EU-C550, and it can be seen through the standard deviation that they may even coincide. This result is contrary to what is expected since besides the porosity of EU-AC being slightly larger. Furthermore, the effect of hydrophobicity should be lower for EU-AC (therefore it should have a higher WHC), since as shown by Gray et.al.[18], there is a decrease of surface functional groups that cause this hydrophobicity, with the increase of the pyrolysis temperature. Anyway, as it was not possible to perform an F-TIR evaluation to these two materials it is not possible to conclude about their surface functionality. On the other hand, looking at PS-C600 and PS-AC, it can be seen that the WHC of PS-AC is 6% higher than PS-C600, which is also true for its porosity.

Regarding the raw biomass, eucalyptus, and pine, both show a high WHC (0.893 and 0.910 cm3 /cm3, respectively), demonstrating well the water absorption capacity of woody biomass. Thus, these results, in addition to substantiate, once again that most of the pores come from the biological structure of biomass itself, it is necessary to consider other phenomena that occur in biomass, the swelling. This is a phenomenon that occurs in biomasses, mainly woody biomasses, due to the expansion of the fibres of the biomass itself, since its stiffness is lower than their respective biochars (in the slow pyrolysis occurs precisely a significant increase of fixed carbon, making the material more rigid). Besides, another effects that are preponderant in the relation of biomass with water is its chemical composition, namely its extractives (non-structural components such as fats, resins, simple sugars, starches, etc.) which can lead to the increase of WHC, and the surface functionality. Due to work limitations, it was not possible to perform the chemical composition of biomass, so the interference of extractives is not possible to quantify.

Thus, considering only the biochars of the respective biomasses, the Pearson's correlation between the WHC and the total pore volume (presents in Table 17) is 0.95, meaning a positive correlation between the WHC and the total pore volume. On the other hand, comparing the results with the specific area determined by BET tests, the Pearson correlation obtained was 0.83 demonstrating that there is no clear correlation between the specific area at nanopore level and the

WHC. These results are in agreement with that presented by Zhang and You[12] , which obtained the same correlation for two different biochars of poplar and pine.

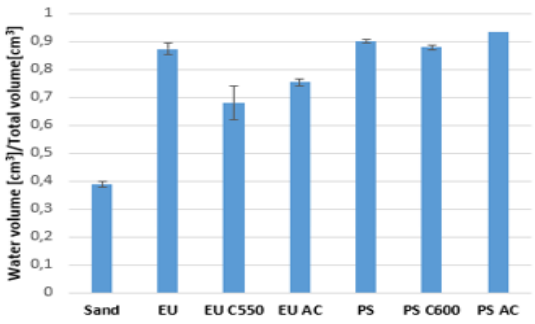


**Figure 11-** Water holding capacity of biomasses on volume basis.

### 3.5. Water retention curves

In this section the retention curves are presented and discussed. The sand curve was used as a control and element mixtures (biomass/biochar) with the sand were considered. Three mixtures (10%,50% and 100% on a volume basis) were made for each element. The experimental points determined were for saturation $\theta_s$, field capacity $\theta_{fc}$ ,$\theta_{pf2.5}$ and wilting point $\theta_{wp}$.

#### 3.5.1. Sand and biochars

The following figures, show the curves for mixtures between sand and biochar. With respect to EU-C550 (figure 12), an increase of 11%, 16%, 48% and 167% for pF points 0, 2, 2.54 and 4.2 for 10% biochar in the mixture with sand is found. Increase of 22%,73%,203% and 667% for pF points 0,2,2.54 and 4.2 for 50% mixing with sand. And increase of 75%, 58%,72% and 21.33% for 100% of EU-C550 for pF points 0.2,2.54 and 4.2. For EU-AC (figure 13), an increase of 10%, 18%, 58% and 67% for pF points 0, 2, 2.54 and 4.2 is found for 10% biochar in the mixture with sand. Increase of 36%,89%,236% and 1967% for pF points 0,2,2.54 and 4.2 for 50% mixing with sand. And increase of 94%, 93%,507% and 5000% for 100% EU-AC for pF points 0,2,2.54 and 4.2.

For PS-C600 (figure 14), an increase of 17%, 14%, 34% and 0% for pF points 0, 2, 2.54 and 4.2 for 10% biochar in the mixture with sand is found. Increase of 56%,95%,173% and 1033% for pF points 0,2,2.5 and 4.2 for 50% mixing with sand. And increase of 126%, 189%,345% and 2667% for 100% of PS-C600 for pF points 0,2,2.54 and 4.2.

The effect of biochar when compared to the sand control is visible. There is also a non-linearity concerning the percentage of element used with the sand, this is due to the fact that there are several parameters that will affect the water retention, namely the interpores between the sand and biomass/biochar particles and the intrapores of the biochar itself.

However as reported by Yi et.al [19], considering the same particle size range for both sand and biochar, the effect of inter-pores is diminished, hence the same size for both elements (400μm to 1mm) was selected for this work. Thus, looking at the values, it can be seen that for biochars there is an increase to $\theta_{fc}$, $\theta_{pF=2.54}$, $\theta_{wp}$ for all biochars due mainly to the intraporous. This is because if capillary potential is the main effect, then capillary forces are the main factor in water retention. These are described by the Young-Laplace equation (equation 7), which indicates that the smaller the pore, the greater the pressure to remove the water from that pore, which agrees with the fact that the water retention values for biochar mixtures at the wilting point are much higher than for sand, since this is the point of greatest pressure and only the smallest pores retain water. However, looking at the formula there is also the effect of the contact angle which depends on hydrophobicity, hence the relationship is not entirely direct between smaller pores and more water retained.

$$P_c = \frac{2\gamma \cos\theta}{r} \qquad (7)$$

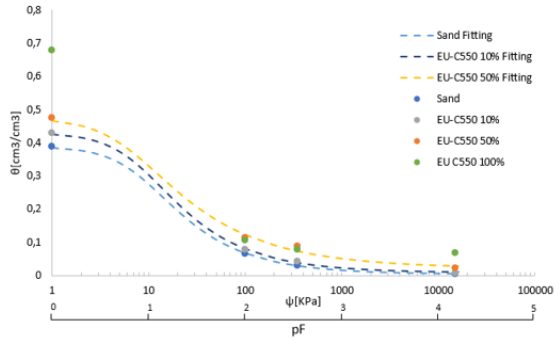


**Figure 12-**WRC for sand, EUC-C550 at 10%,50% and 100%.

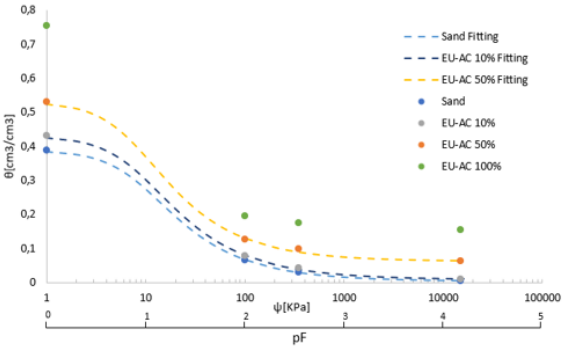


**Figure 13-** WRC for sand, EU-AC at 10%,50% and 100%.

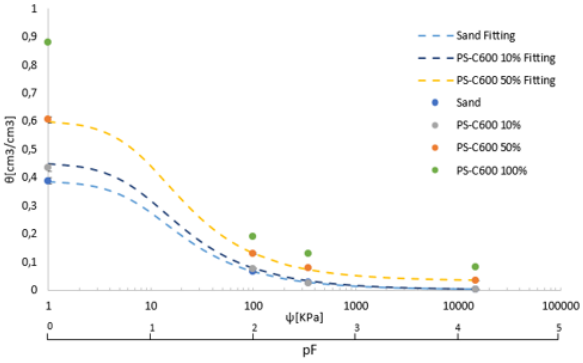


**Figure 14-** WRC for sand, PS-C600 at 10%,50% and 100%.

### 3.5.2. Sand and biomasses

In relation to pine biomass (figure 15), PS-Raw, there is an increase of 12%, 17%, reduction of 13% and change of 0% for pF points 0, 2, 2.54 and 4.2 for 10% biomass in the mixture with sand. Increase of 46%,75%,328% and 1233% for pF points 0,2,2.54 and 4.2 for 50% mixing with sand. And increase of 132%, 157%,469% and 3433% for 100% PS-Raw for pF points 0, 2, 2.54 and 4.2.

Considering EU-Raw (figure 16) there is an increase of 11%, 22%,75% and 67% for pF points 0, 2, 2.54 and 4.2 for 10% biomass in the mixture with sand. Increase of 51%,108%,261% and 1733% for the points of pF 0,2,2.54 and 4.2 for 50% of mixture with sand. And increase of 125%, 205%,483% and 4200% for 100% EU-Raw for pF points 0, 2, 2.54 and 4.2. Thus, it can be observed that an increase occurs for all points comparing only with the isolated sand, taking away a value for PS-Raw for pF 2.54 that could represent an outlier. However, although it has been concluded that much of the larger scale pores come from the biological structure of the biomass, it is difficult to correlate this water retention with the porosity of the material alone for several reasons. One of them, as already mentioned in sub-section 4.4, is the fact that there is the phenomenon of swelling that is always difficult to quantify since it is due to the expansion of biomass fibres. On the other hand, the extractives can also have a significant effect. And lastly, since raw biomass is not a very rigid structure unlike biochar, pore deformation may occur when pressure is applied. However, it is also noted that biomass has a positive response in terms of water retention when mixed with sand, which is not generally considered as an object of study in the literature.

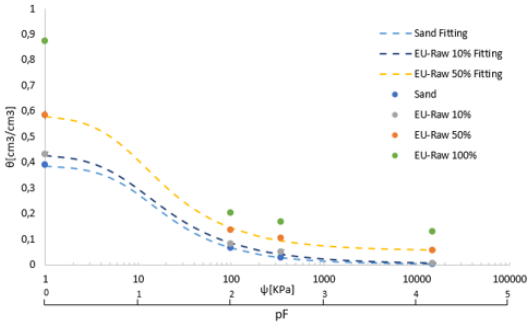


**Figure 15-** WRC for sand, EU-Raw at 10%,50% and 100%.

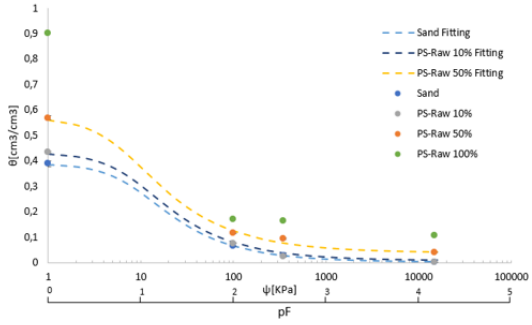


**Figure 16-** WRC for sand, PS-Raw at 10%,50% and 100%

### 3.5.3. Plant available water

To study the effect of biomass/biochar from the point of view of practical application, another parameter is introduced which is called the available water for plants $\theta_{paw}$, and is determined according to equation 8:

$$\theta_{paw} = \theta_{fc} - \theta_{wp} \quad (8)$$

where $\theta_{fc}[\frac{cm^3}{cm^3}]$ is the field capacity and $\theta_{wp}[\frac{cm^3}{cm^3}]$ is the wilting point.

In Table 5, is present the summary of the parameters for all mixtures and materials, so it can be seen that the material that has higher $\theta_{paw}$ is the PS-C600 at 100% (71% higher) with a value of 0.1080 [cm3/cm3], however only two materials have a plant available water lower than the sand, which are EU-AC and EU-C550 as elements (without mixing), due to the fact that the amount of water retained at the wilting point is still high due to water retention in the intra-pores, leading to the fact that the available water between the field capacity and the wilting point is not high. This leads to the conclusion that the use of biochar has to be considered, because if it is used in a high percentage the retention value for the wilting point can be so high that it makes the value of plant available water lower than that of sand alone. However, it is not feasible to apply 100% biochar in a practical way, so it is also necessary to quantify which would be the best with the mixtures in function of the percentages. Thus, a 50% mixture of PS-C600 improves 50% over sand, while a 10% mixture improves 16%. The EU-C550 improves 45% and 9% in a mixture at 50% and 10%, respectively. As for biomasses, PS-Raw improves 19% and 17% in a 50% and 10% mixture, respectively. While EU-Raw improves 31% and 20% in a mixture of 50% and 10%, respectively.

**Table 5 –** Plant available water for mixtures with sand and biomass/biochar

| Category | Volume | Sample | $\theta_{paw}[cm^3/cm^3]$ |
|---|---|---|---|
| **Mixtures** | | **Sand** | 0.0632 |
| **Mixtures** | **10%** | **EU Raw** | 0.0757 |
| **Mixtures** | **10%** | **PS-Raw** | 0.0742 |
| **Mixtures** | **10%** | **PS-C600** | 0.0735 |
| **Mixtures** | **10%** | **EU-AC** | 0.0731 |
| **Mixtures** | **10%** | **EU-C550** | 0.0690 |
| **Mixtures** | **50%** | **PS-C600** | 0.0950 |
| **Mixtures** | **50%** | **EU-C550** | 0.0916 |
| **Mixtures** | **50%** | **EU Raw** | 0.0825 |
| **Mixtures** | **50%** | **PS-Raw** | 0.0756 |
| **Mixtures** | **50%** | **EU-AC** | 0.0632 |
| **Elements** | **100%** | **PS-C600** | 0.1080 |
| **Elements** | **100%** | **EU Raw** | 0.0728 |
| **Elements** | **100%** | **PS-Raw** | 0.0643 |
| **Elements** | **100%** | **EU-AC** | 0.0409 |
| **Elements** | **100%** | **EU-C550** | 0.0378 |

## 4.Conclusions

In this work were considered two biomasses pine and eucalyptus. Through slow pyrolysis processes (laboratory and industrial) biochars and activated biochars were obtained. With the characterisation of the biomass/biochars, in order to analyse their pore structure, it is concluded that for pores higher than nanopores, a great influence comes from the biological structure of the raw biomass. While for pores below 4 nm (BET), the effect of activation ($937 m^2 g^{-1}$) is clear. On the other hand, it is concluded that biochar has a positive influence on water retention when mixed in sandy soils. An increase in retention was verified for all pressure points, with special focus on the highest-pressure point (wilting point), which shows the clear effect of intra-pores. Furthermore, it is a phenomenon that depends on several factors, proving that there is no linearity in retention between the 10% to 100% volume bases. In practical terms, considering the water available to the plants (it depends on the field capacity and the wilting point), the use of biochar should be considered so that the wilting point is not too high. Finally, the raw biomasses also showed favourable results.

## 5.References


[1] M. A. Perea-Moreno, E. Samerón-Manzano, and A. J. Perea-Moreno, "Biomass as renewable energy: Worldwide research trends," *Sustain.*, vol. 11, no. 3, pp. 1–21, 2019, doi: 10.3390/su11030863.

[2] P. Basu, "Chapter 1 - Introduction," in *Biomass Gasification, Pyrolysis and Torrefaction (Second Edition)*, Second Edi., P. Basu, Ed. Boston: Academic Press, 2013, pp. 1–27.

[3] P. Basu, "Chapter 5 - Pyrolysis," in *Biomass Gasification, Pyrolysis and Torrefaction (Second Edition)*, Second Edi., P. Basu, Ed. Boston: Academic Press, 2013, pp. 147–176.

[4] F. Ronsse, R. W. Nachenius, and W. Prins, *Carbonization of Biomass*. Elsevier B.V., 2015.

[5] J. Lehmann and S. Joseph, "Biochar for environmental management: Science and technology," *Biochar Environ. Manag. Sci. Technol.*, pp. 1–416, 2012, doi: 10.4324/9781849770552.

[6] J. Lehmann, "Bio-energy in the black," *Front. Ecol. Environ.*, vol. 5, no. 7, pp. 381–387, 2007, doi: 10.1890/1540-9295(2007)5[381:BITB]2.0.CO;2.

[7] J. H. Windeatt, A. B. Ross, P. T. Williams, P. M. Forster, M. A. Nahil, and S. Singh, "Characteristics of biochars from crop residues: Potential for carbon sequestration and soil amendment," *J. Environ. Manage.*, vol. 146, pp. 189–197, 2014, doi: 10.1016/j.jenvman.2014.08.003.

[8] M. Carrier, T. Hugo, J. Gorgens, and H. Knoetze, "Comparison of slow and vacuum pyrolysis of sugar cane bagasse," *J. Anal. Appl. Pyrolysis*, vol. 90, no. 1, pp. 18–26, 2011, doi: https://doi.org/10.1016/j.jaap.2010.10.001.

[9] A. K. Sakhiya, A. Anand, and P. Kaushal, *Production, activation, and applications of biochar in recent times*, vol. 2, no. 3. Springer Singapore, 2020.

[10] J. Zhang, Q. Chen, and C. You, "Biochar Effect on Water Evaporation and Hydraulic Conductivity in Sandy Soil," *Pedosphere*, vol. 26, no. 2, pp. 265–272, 2016, doi: 10.1016/S1002-0160(15)60041-8.

[11] D. A. Laird, P. Fleming, D. D. Davis, R. Horton, B. Wang, and D. L. Karlen, "Impact of biochar amendments on the quality of a typical Midwestern agricultural soil," *Geoderma*, vol. 158, no. 3, pp. 443–449, 2010, doi: https://doi.org/10.1016/j.geoderma.2010.05.013.

[12] J. Zhang and C. You, "Water holding capacity and absorption properties of wood chars," *Energy and Fuels*, vol. 27, no. 5, pp. 2643–2648, 2013, doi: 10.1021/ef4000769.

[13] J. Parikh, S. A. Channiwala, and G. K. Ghosal, "A correlation for calculating HHV from proximate analysis of solid fuels," *Fuel*, vol. 84, no. 5, pp. 487–494, 2005, doi: 10.1016/j.fuel.2004.10.010.

[14] S. Bikbulatova, A. Tahmasebi, Z. Zhang, S. K. Rish, and J. Yu, "Understanding water retention behavior and mechanism in bio-char," *Fuel Process. Technol.*, vol. 169, no. September 2017, pp. 101–111, 2018, doi: 10.1016/j.fuproc.2017.09.025.

[15] A. Fong, "Determination of Soil Water Characteristic Curve Using 5 Bar Ceramic Pressure Plate Extractor," vol. 1, 2018.

[16] M. T. van Genuchten, "A Closed-form Equation for Predicting the Hydraulic Conductivity of Unsaturated Soils," *Soil Sci. Soc. Am. J.*, vol. 44, no. 5, pp. 892–898, 1980, doi: https://doi.org/10.2136/sssaj1980.03615995004400050002x.

[17] Y. Chun, G. Sheng, G. T. Chiou, and B. Xing, "Compositions and sorptive properties of crop residue-derived chars," *Environ. Sci. Technol.*, vol. 38, no. 17, pp. 4649–4655, 2004, doi: 10.1021/es035034w.

[18] M. Gray, M. G. Johnson, M. I. Dragila, and M. Kleber, "Water uptake in biochars: The roles of porosity and hydrophobicity," *Biomass and Bioenergy*, vol. 61, pp. 196–205, 2014, doi: 10.1016/j.biombioe.2013.12.010.

[19] S. Yi, N. Y. Chang, and P. T. Imhoff, "Advances in Water Resources Predicting water retention of biochar-amended soil from independent measurements of biochar and soil properties," vol. 142, no. February 2019, 2020, doi: 10.1016/j.advwatres.2020.103638.